

*Letter to the Editor***Very cold dust in the peculiar dwarf elliptical galaxy NGC 205*****Martin Haas**

Max-Planck-Institut für Astronomie (MPIA), Königstuhl 17, D-69117 Heidelberg, Germany

Received 16 June 1998 / Accepted 27 June 1998

Abstract. ISO observations of NGC 205 between 120 and 200 μm resolve the emission from 20–24 K cold dust. It is extended to about $7'.5 \times 7'.5$ with bright concentrations in a $1'.5$ north-south elongated area, similar to the that seen in HI. Supplemented by IRAS and mm literature data, the photometry of the total galaxy and the central region is disentangled. It indicates the presence of very cold dust below 10 K which would be the first such detection in an elliptical galaxy.

Key words: infrared: galaxies – galaxies: elliptical, peculiar, photometry – fundamental parameters – individual: NGC 205

1. Introduction

NGC 205, one of the companions of M31, is classified as peculiar dE5. It shows a dozen bright early type stars and dark clouds, hence signatures of recent star formation (Hodge 1973). The HI emission is extended to about $3'$ (Young and Lo 1997). NGC 205 was also detected by IRAS at 12–100 μm with a spectral energy distribution steeply rising between 60 and 100 μm (Rice et al. 1988, Knapp et al. 1989) indicating the presence of cool dust at a temperature around 25 K and a slight extension at 60 and 100 μm along $\text{PA} = -47^\circ$. NGC 205 is also the first among all ellipticals which was detected at the 1.1mm continuum (Fich and Hodge 1991).

Here new ISO observations between 120 and 200 μm are presented bridging the spectral energy distribution between IRAS and mm range and addressing the extension of the dust emission.

2. Observations and Data Reduction

The observations were performed on 15th Dec 1997 with the C200 array of ISOPHOT (Lemke et al. 1996), the photometer on board ISO (Kessler et al. 1996). Raster maps at 120, 150, 180 and 200 μm , each $13'.5 \times 13'.5$ in size and centered on $\alpha_{2000} =$

$0^{\text{h}}40^{\text{m}}22.0^{\text{s}}$, $\delta_{2000} = +41^\circ 41' 26''$, were obtained with a sampling of $1'.5$. Since this is also the pixel size of the 2×2 array, each pixel provides a complete map of the galaxy (except of the border), thus avoiding flatfield problems, and the 4-fold redundancy increases the stability against artefacts like relicts of cosmic glitches. The total integration time per sky pixel was 64 s at 200 μm and 48 s at the other more sensitive filters.

The data were reduced using the PHT Interactive Analysis tool (PIA¹) V7.1 in standard processing mode, together with the calibration data set V4.0 (Laureijs et al. 1998). This includes correction for the electronics' non-linearity, deglitching (removal of data sections disturbed by cosmic particle events), correction for signal dependence on the reset time interval. The detector responsivity was calibrated using associated measurements of the thermal fine calibration source on board.

The accuracy of the absolute photometric calibration depends mainly on systematic errors like those from detector transients and responsivity drifts, and it is currently known to be better than 30%. In fact, at each filter the deviations between the four independent maps obtained by the four detector pixels reached about 10% in the overlapping areas, and the average of the four maps was taken for the final map. Also, since the observations were performed directly one after another, the relative filter to filter calibration relevant for the shape of the SEDs should be better than 10% which is the upper limit of the formal errors as well. Finally, differential details within the maps are accurate to better than 5%.

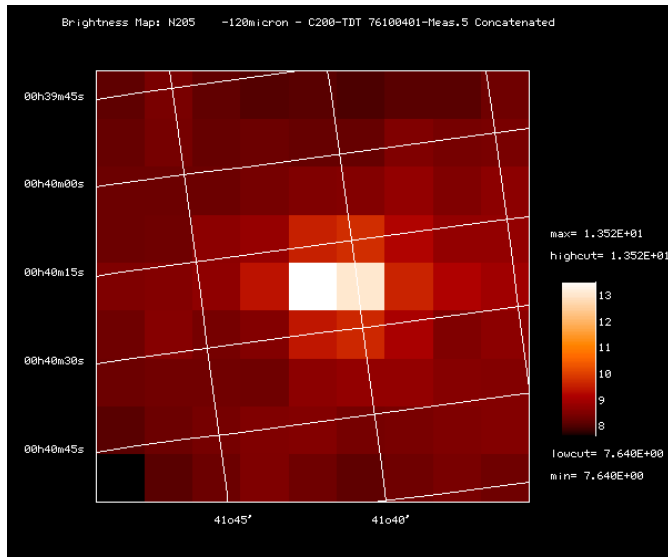
3. Results and Discussion

Fig. 1 shows the ISO raster maps at 120 and 200 μm , those at 150 and 180 μm look very similar. At the spatial resolution of $1'.5$ most of the emission is seen by two pixels, the central one and its southern neighbour. The footprint (120 μm : $d_{\text{Airy}} = 101''$, $d_{\text{FWHM}} = 42''$; 200 μm : $d_{\text{Airy}} = 168''$, $d_{\text{FWHM}} = 70''$) is larger than the pixel size of $90''$ and the pointing accuracy of the ISO satellite is better than $5''$. First we examine, how far the emission could originate from a point source located near the border between the two pixels. Then the point source flux should

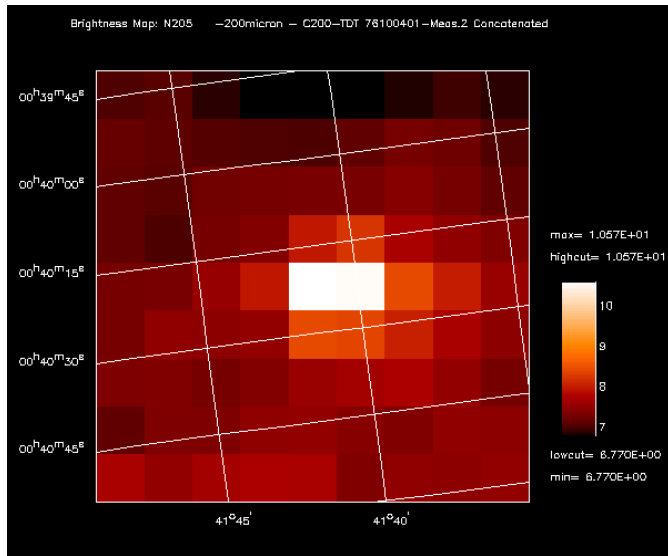
Send offprint requests to: M. Haas (e-mail: haas@mpia-hd.mpg.de)

* Based on observations with ISO, an ESA project with instruments funded by ESA Member States (especially the PI countries: France, Germany, the Netherlands and the United Kingdom) and with the participation of ISAS and NASA.

¹ PIA is a joint development by the ESA Astrophysics Division and the ISOPHOT Consortium led by the MPIA. Contributing Consortium institutes are DIAS, RAL, AIP, MPIK, and MPIA.



a



b

Fig. 1a and b. ISO raster maps of N4G205 at $120\ \mu\text{m}$ (top) and $200\ \mu\text{m}$ (bottom). North is about left. The pixel size is $1''.5$. The color table gives surface brightness in [MJy/sr]. Note the cross-like pattern of the footprint around the two bright pixels.

be roughly the sum of their flux around 2 Jy. Since the ISO serendipity survey with the C200 detector could undoubtedly detect 2 Jy sources from much faster slews across the sky (Bogun et al. 1996, Stickel et al. 1998), a point source would be bright enough to show up as a clear peak in the signal time series, when the telescope slewed between the two raster positions. But we could not find such a peak as is illustrated in Fig. 2. Therefore we are convinced that the flux seen by the two bright pixels does not originate from a point source between them, rather it is due to resolved emission.

Fig. 3 illustrates the location of the two bright ISO map pixels with respect to the HI contours. While the central pixel

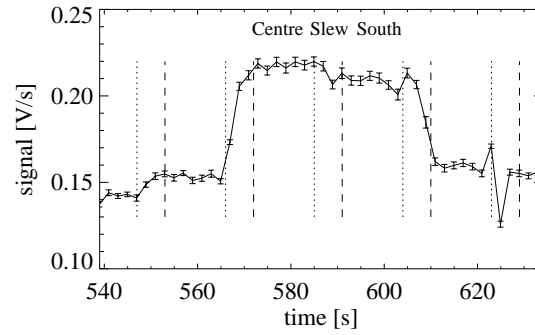


Fig. 2. Signal time series at $120\ \mu\text{m}$ (pixel 2) illustrating the signal transient during the satellite slews between the raster points. The start and end of a slew are marked by the dotted and dashed vertical lines. The signal immediately increases when slewing (from North) onto the center, and similarly decreases when leaving the southern raster point. Since there is no increase when slewing from the central to the southern pixel, this refutes the possibility that the emission comes from a point source located between the two raster positions.

Table 1. Isophot photometry of NGC 205 and resolved components (*uncorrected* gives the flux of the single pixel *before* footprint correction, *extended ring* = *total* - *center* - *south*). The fluxes are in Jy. The errors are about 10% of the quoted fluxes.

component	area	wavelength			
		120 μm	150 μm	180 μm	200 μm
total	$7''.5 \times 7''.5$	5.41	5.53	4.66	4.15
intermediate part	$4''.5 \times 4''.5$	3.85	3.66	3.05	3.04
center uncorrected	$1''.5 \times 1''.5$	1.23	1.09	0.87	0.80
center	$1''.5 \times 1''.5$	1.55	1.57	1.23	1.08
south uncorrected	$1''.5 \times 1''.5$	1.05	1.04	0.84	0.80
south	$1''.5 \times 1''.5$	1.35	1.44	1.16	1.08
extended ring		2.51	2.52	2.27	1.99

covers the galaxy nucleus and the HI peak (\approx cloud 11) north of it (both also measured at 1.1 mm by Fich and Hodge, 1991), the bright HI maximum south of the nucleus coincides with the southern pixel. Thus the dust emission might be correlated with the HI emission.

Fig. 4 shows the cuts through the ISO maps along north-south direction. They further reveal that, while at 120 and 150 μm the center constitutes the brightest peak, at 180 and 200 μm the southern region reaches similar brightness as the center. This indicates that the center of NGC 205 is slightly warmer than the southern region.

Photometry was derived for the total galaxy as well as the center and the southern region, taking the outer map parts (2 pixels = $3'$ wide) for background subtraction. The total flux is estimated from the inner $7''.5 \times 7''.5$ (5×5 pixels), and the center and southern flux from the central and the southern pixel alone applying a footprint correction and accounting for the reciprocal contributions. The fluxes are listed in Table 1. Remarkably about 40–50% of the total flux comes from the extended ring area outside the (footprint corrected) central and southern regions, but

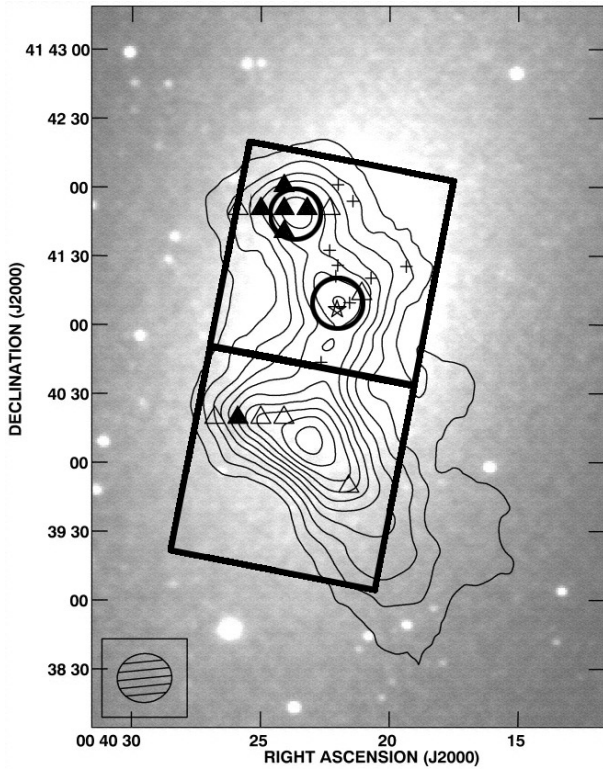


Fig. 3. Location of the two bright pixels of the ISO maps overlaid as thick 90'' squares on the HI contour map from Young and Lo (1997). The two pixels nicely cover the regions around the nucleus and the southern HI emission. Also, the 18'' beam of the 1.1 mm observations of the nucleus and cloud 11 by Fich and Hodge (1991) is shown as thick circle within the central ISO pixel. (The small crosses and triangles indicate regions of special interest in the paper by Young and Lo. The filled triangles give locations of CO detections.)

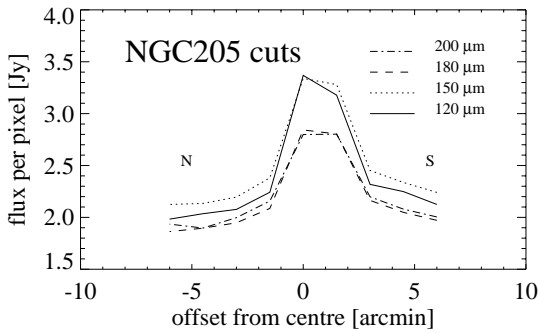


Fig. 4. North-South cuts through the ISO maps.

within 7.5×7.5 . Also, the intermediate part of 4.5×4.5 yields fluxes between the total one and the sum of the central and southern regions giving further support for a substantial contribution by extended dust. Attempts to integrate the flux over larger areas than 7.5 yielded no increase, but became more noisy, because of improper background determination. Though there could be more far extended flux, our total flux from 7.5×7.5 might well approximate the ultimate one.

Fig. 5 shows the spectral energy distribution for the total galaxy and the center supplemented by IRAS and mm data. The

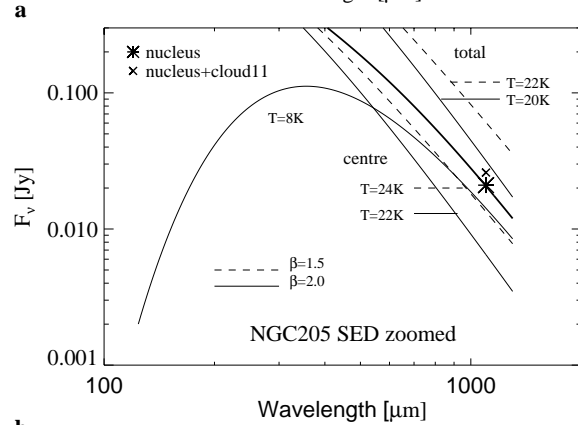
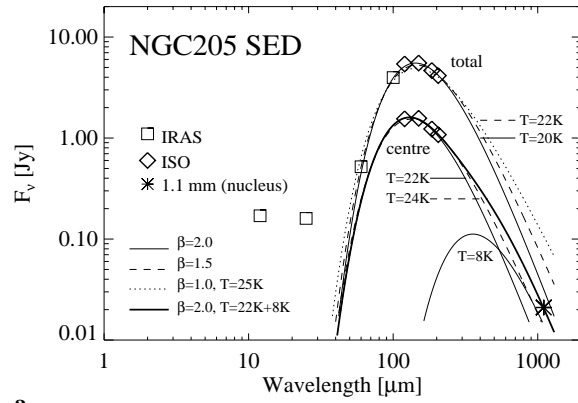


Fig. 5a and b. *Top:* Spectral Energy Distributions for the total galaxy and the center. The errors are about the size of the symbols. The lines represent $\lambda^{-\beta}$ power-law modified blackbodies. *Bottom:* Zoomed portion around 1100 μm .

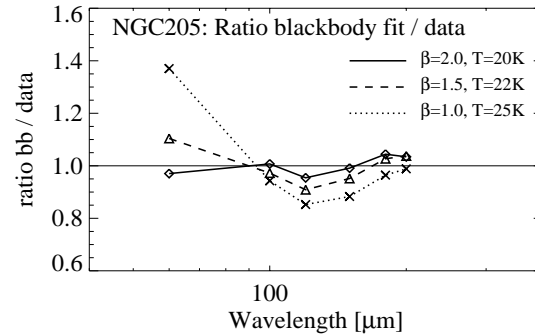


Fig. 6. Ratios of the fitted blackbodies to the measured total fluxes for several values of the emissivity exponent β . Ideally the ratios should be unity at all wavelengths. $\beta = 2$ provides the best fit to the data.

ISO measurements now clearly reveal the maximum of the SED around 120–150 μm and the Rayleigh-Jeans decline longward thereof. In order to characterise the dust emission, $\lambda^{-\beta}$ power-law modified blackbody curves are considered with emissivity exponent $\beta = 1, 1.5$ and 2 . With $\beta = 1.5$ and 2 the ISO and IRAS data points are nicely fitted and the effect of β rather shows up longwards of 200 μm . Fig. 6 shows the deviation of the fits from the IRAS and ISO data for the total galaxy. The shallow $\beta = 1.0$ provides the worst fit, and $\beta = 2.0$ appears

Table 2. Dust temperature, luminosity ($L_{\text{FIR}} = L_{40-1100\mu\text{m}}$) and mass for NGC 205 and the resolved components, derived from the blackbody curves shown in Fig. 5. The second component for the center at 8 K refers to a 1.1 mm flux of 7 and 19 mJy at $\beta = 1.5$ and 2, resp.

component	$\beta = 1.5$			$\beta = 2.0$		
	T K	L_{FIR} $10^4 L_{\odot}$	M M_{\odot}	T K	L_{FIR} $10^4 L_{\odot}$	M M_{\odot}
total	22	230	4030	20	210	4890
center	24	73	780	22	70	880
center, comp. 2	8	2	2100	8	2	11800
south	22	57	1020	20	55	1230
extended	22	107	1910	20	103	2320

somewhat closer to the data than $\beta = 1.5$. Therefore we reject $\beta = 1.0$ and restrict the further discussion to $\beta = 1.5$ and 2. The value of β plays a crucial role for interpretations and is still a matter of debate. Exact observational determination remains difficult, since most sources exhibit a mixture of various dust temperatures. While moderate approaches prefer the shallower value of $\beta = 1.5$ (and sometimes even $\beta = 1.0$), more and more observational examples are found favoring the steeper value of $\beta = 2$ for the typical interstellar dust at temperatures between 20 and 50 K (e.g. Chini et al. 1995, Lehtinen et al. 1998). Since we can not definitely decide on β for NGC 205, we discuss the data for both cases.

As zoomed in Fig. 5 (bottom), for the total galaxy both $\beta = 1.5$ and 2 yield extrapolated 1.1 mm fluxes (61 and 31 mJy) which are clearly above the one measured for the nucleus (21 mJy). This provides compelling evidence for additional 1.1 mm flux from outside of the nucleus, the missing flux must be the higher the shallower β is. Since the mm beam was smaller than the ISO beam, one should try to obtain a more realistic 1.1 mm flux estimate which compares better to the ISO center. Simply scaling up the measured mm flux proportional to the five times larger area would yield about 100 mJy which appears somewhat high and arbitrary. Therefore we consider the 5 mJy observations of cloud 11 (though not a 3σ detection, Fich and Hodge, 1991), which coincides with the HI emission north of the nucleus and is also covered in the ISO center pixel (Fig. 2). Then nucleus and cloud 11 together give a 1.1 mm flux of $21 + 5 = 26$ mJy which may still represent a lower limit for the center. $\beta = 1.5$ as well as $\beta = 2$ yield extrapolated fluxes for the center (15 and 7 mJy) clearly below the one for the nucleus and cloud 11. If $\beta = 2$, then the discrepancy ($26 - 7 = 19$ mJy) is large enough to infer already the existence of an additional component of very cold dust. But also for the case $\beta = 1.5$ the discrepancy ($26 - 15 = 11$ mJy) since a lower limit suggests an additional component of very cold dust. A component with a

temperature of 8 K would ideally fulfill this requirement. The one shown in Fig. 5 has a 1.1 mm flux of 14 mJy ($\beta = 2$). A component warmer than 10 K would show up at $200 \mu\text{m}$.

Table 2 lists the derived dust parameters for the blackbody curves in Fig. 5. The dust mass was estimated with the same formula (2) and basic dust grain assumptions as stated by Fich and Hodge (1991). For comparison they predicted a temperature between 20 and 26 K depending on the emissivity and give a lower limit for the dust mass of about $3000 M_{\odot}$ for $\beta = 2$. Despite the rough agreement of their and our temperature and mass estimates for the cold dust which lead to similar conclusions about the extinction and clumpiness of the dust allocations, the main advantage of the new ISO measurements consists of measuring the SED at its maximum and of spatially separating the center, allowing to infer for the first time the presence of very cold dust below 10 K in an elliptical galaxy. Since the very cold dust is derived in the center of NGC 205, it is likely to find a larger fraction outside as well. For comparison, in the late type Andromeda galaxy very cold molecular clouds have been detected via CO observations by Allen and Lequeux (1993). The nature of very cold dust is quite unknown. Probably it has larger grain sizes up to $1 \mu\text{m}$, like found in the solar system with the ULYSSES satellite (Grün et al. 1994). Further submm and mm observations should be able to extend the conclusions beyond the finding of the existence of very cold dust in NGC 205 reported in this letter.

Acknowledgements. It is a pleasure to thank the teams at the ISOPHOT Data Centre in Heidelberg, Germany, and the ISOPHOT Instrument Dedicated Team in Villafranca, Spain, in particular Uwe Herbstmeier, Bernhard Schulz and Ulrich Klaas for their extreme engagement in the calibration and scientific validation of the instrument. The development and operation of ISOPHOT and the data reduction are supported by funds from Deutsches Zentrum für Luft- und Raumfahrt (DLR, formerly DARA).

References

- Allen R.J., Lequeux J., 1993, ApJL 410, L15
 Bogun S., Lemke D., Klaas U., et al., 1996, A&A 315, L71
 Chini R., Krügel E., Lemke R., et al. 1995, A&A 295, 317
 Fich and Hodge, 1991, ApJL 374, L17
 Grün E., Gustafson B., Mann A., et al. 1994, A&A 286, 915
 Hodge 1973, ApJ 182, 671
 Kessler M.F., Steinz J.A., Anderegg M.E., et al., 1996, A&A 315, L27
 Knapp G.R., Guhathakurta P., Kin D.W., Jura M., 1989, ApJS 70, 329
 Laureijs R. et al., 1998, ISOPHOT Data User Manual, V4.0
 Lehtinen K., Lemke D., Mattila K., et al. 1998, A&A 333, 702
 Lemke D., Klaas U., Abolins J., et al., 1996, A&A 315, L64
 Stickel M., Bogun S., Lemke D., et al., 1998, A&A, 336, 116
 Rice W., Lonsdale C.J., Soifer B.T., et al. 1988, ApJS 68, 91
 Young and Lo 1997, ApJ 476, 131